Unravelling the kinematics of the Brewer-Dobson circulation change

P. Šácha[1], R. Zajíček[1,4], A. Kuchař[2], R. Eichinger[1,3], P. Pišoft[1], H. E. Rieder[2]

[1]Department of Atmospheric Physics, Faculty of Mathematics and Physics, Charles University; V Holešovičkách 2, 180 00 Prague 8, Czech Republic.
[2]Institute of Meteorology and Climatology, University of Natural Resources and Life Sciences, Vienna (BOKU); Gregor-Mendel-Strasse 33, 1180 Vienna, Austria.
[3]Deutsches Zentrum für Luft- und Raumfahrt (DLR), Institut für Physik der Atmosphäre, Münchener Strasse 20, 82234 Weßling, Germany.
[4]Institute of Atmospheric Physics CAS, 14100 Prague, Czech Republic.

Key Points:

- Tropical upwelling is sensitive to various climate change-induced processes, including changes in vertical and horizontal atmospheric structure.
- The width of the upwelling region is highlighted as a very uncertain and potentially important contribution to the circulation change.
- Larger spread is found among the reanalyses than models regarding the net upwelling and individual contribution changes.

Corresponding author: Petr Šácha, petr.sacha@matfyz.cuni.cz

Abstract

Climate models robustly project acceleration of the Brewer-Dobson circulation (BDC) in response to climate change. However, the BDC trends derived from comprehensive models do not fully match observations. Additionally, the changing structure of the troposphere and stratosphere has received increasing attention in recent years and to which extent vertical shifts of the circulation are driving the acceleration is under debate. In this study, we present a novel method that enables the attribution of circulation changes to individual kinematic factors. Using this method allows to study the advective BDC trends in unprecedented detail and sheds new light into discrepancies between different datasets (reanalyses and models) at the tropopause and in the lower stratosphere. Our findings provide insights into the reliability of model projections of BDC changes and offer new possibilities for observational constraints.

Plain Language Summary

The large-scale interhemispheric meridional overturning circulation in the middle atmosphere determines the composition of this region, including the distribution of radiatively important trace gases. The long term change of this circulation is a subject of ongoing debate, and area of disagreement between models and observations. In our study we present a method that provides an unprecedented insight into the change and disentangles the individual factors behind it. Hence, the method introduces new constraints on the circulation change and can aid the reconciliation between models and observations.

1 Introduction

Changes in atmospheric composition since the preindustrial have substantially warmed surface climate (Ivy et al., 2017) and altered atmospheric structure (Pisoft et al., 2021), temperature (Santer et al., 2023), dynamics, and transport (Eichinger & Šácha, 2020), which in turn affect atmospheric composition. The chemical makeup of the middle atmosphere (Andrews et al., 1987), including the distribution and trends of radiatively important gases such as ozone (Karpechko et al., 2018) and water vapor (Randel & Park, 2019), is dynamically governed by the Brewer-Dobson circulation (BDC), the large-scale, interhemispheric, meridional overturning circulation. Analytically, the BDC is commonly defined as consisting of a diffusive (Butchart, 2014) and advective part described by the residual mean circulation (Andrews et al., 1987). Given its importance for atmospheric composition, a realistic representation of the structure, strength, and variability of the BDC is crucial for earth system and chemistry-climate modelling (Abalos et al., 2021).

Comprehensive global climate models unanimously indicate a strengthening of the BDC during recent decades, which is projected to continue and amplify with progressing climate change. In particular, models consistently project that the advective BDC part accelerates in a warming climate (Butchart et al., 2010; Hardiman et al., 2014; Abalos et al., 2021) and that this acceleration dominates changes in atmospheric composition of the middle atmosphere in projections throughout the 21st century (Butchart, 2014). However, recent BDC trends diagnosed from model fields are not fully matching observations (Stiller et al., 2017). Moreover, there is evidence that not only changes in CO_2 and CH_4 abundances but also ozone depleting substances are key drivers of the BDC trends (Polvani et al., 2018). Taken together, the robustness of the modelled changes, past and future, are associated with uncertainties und thus represent a topic of ongoing research and debate within the scientific community.

In studies investigating BDC changes, a frequently explored proxy for the advective BDC component is the net tropical upwelling across the 70 hPa (Butchart et al., 2010), 100 hPa (Abalos et al., 2021) isobars or the tropopause (Ortland & Alexander, 2014), which quantifies the amount of air mass advected by the residual mean circulation from the troposphere into the stratosphere and beyond.

Another robust impact of changes in atmospheric composition is the changing vertical structure of the atmosphere. While the troposphere is warming and thermally expanding (Santer et al., 2003; Vallis et al., 2014), the stratosphere is cooling and contracting (Pisoft et al., 2021), which contributes also to changes in the mesosphere and above that undergo a downward shift of pressure levels (Lübken et al., 2013; Solomon et al., 2018). It has been shown that these changes in atmospheric vertical structure interfere with the diagnosed BDC trends (Shepherd & McLandress, 2011; Šácha et al., 2019; Eichinger & Šácha, 2020). Among others it has been illustrated that no robust increase can be detected in the net tropical upwelling when heuristically accounting for the tropopause rise (Oberländer-Hayn et al., 2016). Moreover, the horizontal structure of the tropospheric (Staten et al., 2020) and stratospheric (Hardiman et al., 2014) circulation is also changing, which might affect BDC trends (Stiller et al., 2017) and thus make causal attribution of potential BDC trends an even trickier task. Taken together, these findings motivate the central research question we aim to contribute to here, namely, is the advective BDC component increasing, moving upwards, or are the underlying mechanisms of advective BDC changes even more complex? Unraveling the role of individual factors for BDC change, and quantifying their contribution, could aid reconciling the disagreement between observations and models regarding BDC trends in the (recent) past (WMO, 2018) and enhance confidence in future projections of BDC changes by global chemistry-climate (CCMs) and earth system models (ESMs).

The paper is structured as follows. First we derive the method for decomposition of the BDC changes and describe the statistical approach and datasets. Then we demonstrate the utility of the method by applying it to the most recent reanalysis dataset and compare the results with state-of-the-art earth system model simulations of the recent past. The results section continues with the extension of the analysis towards projections of future advective BDC changes with increasing anthropogenic emissions. The final section of the paper starts with a discussion of the uncertainty of the advective BDC changes that can be studied in unprecedented detail using the decomposition method together with our statistical approach, which is documented in a comparison between multimodel and multireanalysis results for the recent past changes. The paper is concluded by the summary of the results and an outlook of future research directions.

2 Methods and Data

Here we present a methodological framework rooted in environmental fluid mechanics that allows us to quantify the role of the individual aforementioned factors behind the advective BDC changes. In a nutshell our approach is centered around the decomposition of the change in mass transport across time-variable material lines. This allows us to derive the complete set of mechanisms contributing to the net tropical upwelling, and changes therein. Given the kinematic nature of the problem, the solution is dependent on the material line under consideration (e.g., the tropopause or individual pressure levels), where the transport is diagnosed. As a hypothetical example, for a certain material line the BDC can be decreasing and moving upwards, while, at the same time, it might be diagnosed for another to increase and move downwards.

For studying the long term changes in BDC strength, it is advantageous to define a single scalar indicator for this, either the net upwelling or downwelling mass flux across a specified level. Here, we are concerned with the net upwelling across traditional pressure levels (100 and 70 hPa) and across the tropopause. The zonal mean tropopause (TPP) and also the zonal mean isobars define parameterized curves in the z, φ plane with a time-variable location and shape, $\overline{z}(t,\varphi)$. The advective zonal mean mass transport across an oriented element of the zonal mean curve, represented by a vector $\mathrm{d}\vec{l}(\overline{z}(t,\varphi),t,\varphi)$, is given as:

$$\mathrm{d}T(\overline{z}(t,\varphi),t,\varphi) = 2\pi a \cos\varphi \overline{\rho}(\overline{v}^*,\overline{w}^*)\cdot\vec{n}\mathrm{d}l, \tag{1}$$

where a is the radius of the spherical Earth, $\overline{\rho} = \overline{\rho}(\overline{z}(t,\varphi),t,\varphi)$ is the zonal mean density at the respective level (itself a function of time t and latitude φ), $\overline{w}^* = \overline{w}^*(\overline{z}(t,\varphi),t,\varphi)$ and $\overline{v}^* = \overline{v}^*(\overline{z}(t,\varphi),t,\varphi)$ are the vertical and meridional residual mean velocity components evaluated at the respective zonal mean levels, $\vec{n}(\overline{z}(t,\varphi),t,\varphi)$ is a normal vector of the oriented element of

the zonal mean curve and $\mathrm{d}l(\overline{z}(t,\varphi),t,\varphi)$ is the length of the zonal mean curve element. As the location, length and shape (quantified by the angle α it makes with the horizontal) of the zonal mean curves vary with time, the problem is analogous to the computation of transport across a material line.

The net zonal mean advective transport across the selected material line is then computed as an integral of $\mathrm{d}T$ from the South to the North pole along the line and is approximately zero from continuity. However, studying the residual mean circulation associated mass flux in individual upwelling and downwelling branches separately, allows to assess potential changes of this circulation. For this, first, we determine the time varying boundaries between the upwelling and downwelling regions (φ_1, φ_2) as latitudes with the zeroth zonal mean advective transport across the material line. Then we compute the upwelling (U) across the material line L_m as:

$$U(L_m,t) = \int_{\varphi_1(t)}^{\varphi_2(t)} \mathrm{d}T(\overline{z}(t,\varphi),t,\varphi). \tag{2}$$

Having the annual-mean time-series of upwelling, we are ready to derive the kinematic factors contributing to its year-to-year change δU, defined as:

$$\delta U = U(L_m, t+\delta t) - U(L_m, t). \tag{3}$$

Differentiating the integral (2), using the Leibniz integral rule, invoking an analogy to the material derivative concept and after some manipulations (for the complete derivation please refer to the Supplementary Text S1), we get on the leading order a complete decomposition of the net upwelling change across any material line in the form:

$$\begin{aligned}
\delta U = {} & \overbrace{\int_{\varphi_2(t)}^{\varphi_2(t+\delta t)} \mathrm{d}T(\overline{z}(t^*,\varphi),t^*,\varphi) - \int_{\varphi_1(t)}^{\varphi_1(t+\delta t)} \mathrm{d}T(\overline{z}(t^*,\varphi),t^*,\varphi)}^{\text{width term}} + \\
& + \overbrace{2\pi a^2 \int_{\varphi_1}^{\varphi_2} \frac{\partial \overline{z}_{str}}{\partial t} \frac{\partial \overline{\rho}(\overline{w}^* + \overline{v}^* \tan\alpha)}{\partial z} \cos\varphi \, \mathrm{d}\varphi \cdot \delta t}^{\text{z term}} + \\
& + \overbrace{2\pi a^2 \int_{\varphi_1}^{\varphi_2} \overline{\rho} \frac{\partial \overline{w}^*}{\partial t} \cos\varphi \, \mathrm{d}\varphi \cdot \delta t}^{\overline{w}^* \text{ term}} + \overbrace{2\pi a^2 \int_{\varphi_1}^{\varphi_2} \tan\alpha \overline{\rho} \frac{\partial \overline{v}^*}{\partial t} \cos\varphi \, \mathrm{d}\varphi \cdot \delta t}^{\overline{v}^* \text{ term}} + \\
& + \overbrace{2\pi a^2 \int_{\varphi_1}^{\varphi_2} \overline{w}^* \frac{\partial \overline{\rho}}{\partial t} \cos\varphi \, \mathrm{d}\varphi \cdot \delta t + 2\pi a^2 \int_{\varphi_1}^{\varphi_2} \tan\alpha \overline{v}^* \frac{\partial \overline{\rho}}{\partial t} \cos\varphi \, \mathrm{d}\varphi \cdot \delta t}^{\varrho \text{ term}} + \\
& + \overbrace{2\pi a^2 \int_{\varphi_1}^{\varphi_2} \frac{\overline{\rho v}^*}{\cos^2\alpha} \frac{\partial \alpha}{\partial t} \cos\varphi \, \mathrm{d}\varphi \cdot \delta t}^{\text{shape term}} .
\end{aligned} \tag{4}$$

The decomposition (4) reveals a complete set of kinematic factors contributing to the net upwelling changes, which are the change in the width of the upwelling region (width term), the vertical shift of the material line (z term), the contributions from the local accelerations of the vertical ($\overline{w}^*$ term) and meridional ($\overline{v}^*$ term) components of the residual mean velocity, the contribution from the local density change (ρ term), and finally the contribution from the change in the local material line inclination (shape term). In Fig. S1, we illustrate, how the mechanisms contribute to the net upwelling changes. While speed and direction of the residual mean circulation, the vertical shift of the respective material line, and density of air at the material line have been considered in isolation and (partial) combination in previous works, our study breaks new ground by proposing a consistent framework also considering the changes in geometrical features of the upwelling region. Similarly, we can decompose the kinematic contributions for downwelling across any "quasi"-material line (e.g., isentropic levels). Although the net upwelling and downwelling changes shall be approximately equal, the relative importance of individual kinematic factors may differ.

The accuracy of our partitioning methodology is easy to validate after its application to data. Simply, one has to compare the net upwelling (left-hand side of the equation (4)) computed directly from the data with its reconstruction from the sum of the right-hand side terms (for discretization of the method for application on discrete datasets please also refer to the Supplementary Text S2). For example, the correlation between the two time series of a directly computed and reconstructed net upwelling across the tropopause yields R=0.99 when computed from ERA5 (Hersbach et al., 2020, see next section) annual mean data, and R=1.0 for the upwelling across the two isobars.

2.1 Data

We analyze annual mean data from three widely used reanalyses: ERA5 (Hersbach et al., 2020), JRA55 (Kobayashi et al., 2015), and MERRA2 (Gelaro et al., 2017). Along with reanalyses, the data from the Coupled Model Intercomparison project Phase 6 (CMIP6) simulations were used. Specifically, for the recent past we use the Atmospheric Model Intercomparison Project (AMIP) CMIP6 simulations and SSP370 (Eyring et al., 2016) simulations for future climate projections. CMIP6 models that have all the necessary outputs required for the proposed analysis (temperature, geopotential height, $\overline{v}^*$, $\overline{w}^*$, and the tropopause height) are CESM2 (Danabasoglu et al., 2020), CESM2-WACCM (Danabasoglu et al., 2020), MRI-ESM2-0 (Yukimoto et al., 2019) for both AMIP and SSP370 and UKESM1-0-LL (Sellar et al., 2020) only for SSP370. For each model the maximum number of available realisations was used. A more detailed information on the individual models is given in Supplementary Table S1.

2.2 Statistical analysis

We adopt the Dynamical Linear Modeling (DLM) regression from Alsing (2019). While Multiple Linear Regression has been considered a standard approach to assess long-term trends of atmospheric time series with a number of issues (e.g. Kuchar et al., 2017), DLM represents a regression framework with the ability of regression coefficients to evolve in time. This allows DLM to assess the non-linear background trend which corresponds better with non-stationary processes in the atmosphere (Laine et al., 2014). For these reasons, DLM has been recently used to estimate trends in ozone in model outputs (Ball et al., 2018; Karagodin-Doyennel et al., 2022) and observational records (Maillard Barras et al., 2022; Bognar et al., 2022; Laine et al., 2014) quite extensively.

We use the Markov chain Monte Carlo (MCMC) method to infer the posterior distributions of the background level, auto-regressive coefficient (AR1) and regression coefficient of the El Niño–Southern Oscillation (ENSO) variability. This method represents Bayesian DLM estimation of model states, parameters and their uncertainties. We input the ensemble mean and spread of individual models into the DLM regression to capture their forced response and model their time-dependent uncertainty. To illustrate the spread/uncertainties across reanalyses and model ensembles, we visualize the probability density functions of the individual contributions to BDC change in violin plots throughout the manuscript. We note, that if the results are illustrated from a multi-model distribution (MMD) perspective this analysis includes 3000 MCMC samples from each model.

We used here the same DLM model as Ball et al. (2018) but without a seasonal cycle. We also increased the variance of the local trend so that the background trend is more variable on shorter timescales since we use ENSO as the only regressor. For the ENSO variability in future CMIP6 simulations, we use the first principal component of the detrended SST anomalies in the tropical belt, 20°S and 20°N (e.g. Berner et al., 2020) from each model. For the ENSO variability in the AMIP simulations, we use the observed ENSO index. The Brewer-Dobson circulation (BDC) and its proxies are explained mostly by internal variability in the tropics (Iglesias-Suarez et al., 2021). We tested multiple configurations, e.g. including QBO regressors, but the results confirm a large dependency of transport terms on ENSO.

3 Results

Here we discuss results for ERA5 first, followed by the discussion of the decomposition of the net tropical upwelling for the available CMIP6 models, which we compare further below also with the other reanalyses (MERRA2, JRA55). In Fig. 1 we show the posterior distribution of the interannunal changes in tropical upwelling (trend) over 1979–2014 for the most recent reanalysis dataset ERA5. This figure clearly illustrates that the sign (and magnitude) of the net upwelling trend is a function of the material line (e.g. upwelling increases at the tropopause and 100 hPa levels, but decreases at 70 hPa). This is a physically plausible result, given that the structure of the circulation and the amount of purely meridional mass flux in between the 100 hPa and 70 hPa levels is changing as well. From the continuity equation the only constraint emerging is that the net upwelling has to be balanced by a net downwelling across a particular material line. Focusing on the occurrence frequency of (negative or positive) year to year upwelling changes (see individual numbers below the plots in Fig. 1) from ERA5 illustrates that, at TPP and the 100 hPa level, an increase in the net tropical upwelling occurred more frequently than a decrease, while the opposite applies for the 70 hPa material line. At 70 hPa, the largest variations can be attributed to the term connected with the vertical component of the residual mean circulation ($\overline{w}^*$). However, its contribution shows large spread and the sign of the changes, though uncertain, is opposed to the decreasing net upwelling. Further partitioning reveals, that the net change is dominated by two factors that (over)compensate the increase via $\overline{w}^*$. These are the narrowing of the upwelling region at 70 hPa and the co-located upward shift of the isobar. As the 70 hPa isobar is moving systematically upwards, this results in sampling of regions with climatologically smaller mass transport due to the exponential decrease of the density with height. At a fixed altitude, however, the density is increasing with time and the positive contribution by the term connected with it slightly damps the effect of the upward shift. The other kinematic factors ($\overline{v}^*$ and shape term) show a negligible systematic influence on the net upwelling trend at this material line.

In contrast, at the 100 hPa material line, increasing $\overline{w}^*$ is much less uncertain and dominating the trend, thus yielding a net positive upwelling, which is only partly compensated by the upward shift and narrowing of the upwelling region. All other terms do not significantly contribute to the net upwelling trend at this material line in ERA5. At TPP (the bottom row of Fig. 1), which is characterized through more complex geometry, the net positive upwelling trend results from competing effects between the different mechanisms. Here all terms contribute with a very similar magnitude, except the density term, which is negligible in this region. Large positive contributions to the net upwelling stem from the widening and the term connected with the accelerating meridional component of the residual mean circulation ($\overline{v}^*$) and the tropopause shape term. As the tropopause gets more inclined, the efficiency of the accelerating $\overline{v}^*$ for cross-tropopause transport further increases. The positive contributions are only partly compensated by the negative contributions from the terms connected with the upward shift of the tropopause and $\overline{w}^*$ (smaller net negative effect).

Having illustrated the contributions of individual factors to upwelling over the recent decades in ERA5, we turn next to the comparison with the CMIP6 model simulations. For the net upwelling, CMIP6 models and ERA5 agree generally well on the positive trend at 100 hPa and the TPP level (one exception is the MRI model which shows a pronounced spread). In contrast, trends of opposite sign are found at 70 hPa, where CESM2 and WACCM are simulating increased upwelling, compared to the decreasing trend in ERA5, and MRI shows no robust systematic change. Applying the decomposition hinges to a contribution of the widening term in ERA5, where the upwelling region becomes narrower at 70 hPa, but the models do not simulate any significant changes (or altered variability) in this metric. Otherwise, the models and ERA5 agree well on the individual contributions from the other terms. At 100 hPa, again CMIP6 models do not reveal any contribution from the widening term, compared to ERA5. This results overall in slightly stronger net upwelling changes in WACCM and CESM2, which otherwise agree well with ERA5 regarding the contributions from the other terms. The MRI model compares well to ERA5 in terms of the net upwelling, but the individual contributions differ strongly. Compared to the other analyzed datasets, MRI shows the smallest changes connected with the $\overline{w}^*$ term that are to a large

Figure 1. Interannual change of the net upwelling and the contributing terms at 70 hPa (top), 100 hPa (middle) and the tropopause (bottom) for the period 1979-2015. The dots in the individual violin plots depict the position of the median and vertical lines represent the 95% credible interval (also called the highest density interval - HDI). The HDI of ERA5 is represented by the persian-pink band. The colored numbers at the bottom denote the percentage of relative occurrence of negative or positive year to year upwelling changes.

degree compensated by the negative contribution from the vertical shift term, which is, in MRI however, much smaller in magnitude compared to CESM2, WACCM and ERA5. Interestingly MRI slightly differs from the other datasets also in the magnitude of another radiatively driven term - the ρ term.

Overall good agreement can be found between CMIP6 models (esp. CESM2 and WACCM) and ERA5 at TPP. Here only MRI shows a large spread with a double peak structure for the net upwelling, more skewed towards negative values. That said, taking into account only the traditional framework, i.e. the contribution from the $\overline{w}^*$ term, also MRI and ERA5 agree well regarding the net negative contribution. Besides this only the strong effect of the TPP shape term in WACCM stands out as different among models and ERA5, and the models agree well regarding the contributions from most other terms. Compared to ERA5 however, the models show a smaller magnitude of the changes in $\overline{v}^*$ and the vertical shift term and, with the exception of MRI, also in the width term.

Although the models do mostly not simulate the systematic contributions from the width term to the changes in net upwelling in contrast to ERA5 (i.e. negative contribution at the isobars and positive at the tropopause), we are cautious to state that the models indeed miss this contribution. It must be noted that different reanalyses do not agree (on the magnitude and sign) in the contribution from this term. A further investigation of this feature is beyond of the scope of the present study and suggested to be explored in subsequent work including also comparison and validation with direct observational estimates on the width of the upwelling regions. For brevity we discuss this point in more detail in the concluding section (see Sec. 4).

In Fig. 2 we turn now to the analysis of projections of future net upwelling changes, for which besides the models discussed so far also output of the UKESM1 model is available. At TPP, pronounced intermodel differences emerge in the contribution to the net upwelling from the $\overline{v}^*$, vertical shift and tropopause shape terms. In contrast strong agreement among the models is found regarding the contribution to net upwelling changes from the $\overline{w}^*$ term and density terms. As a result, MRI and UKESM1 project decreasing net upwelling at TPP while CESM2 and WACCM are indicating a slight tendency towards increased net upwelling.

At the 70 and 100 hPa material lines all models project increasing net upwelling of similar magnitude and with similar variability. Decomposing the net upwelling at 70 hPa into individual factors reveals that the agreement among models stems largely from a compensation between pronounced intermodel differences in contributions resulting from the $\overline{w}^*$ and the upward shift terms. From a conceptual point of view a complete cancellation of the effects of those two terms would emerge, if the changes would originate solely from the shift in the vertical circulation, and no acceleration of the circulation would occur. It is, however, apparent from Fig. 2 that this is clearly not the case at the 70 hPa material line, given that in absolute terms the contribution from the $\overline{w}^*$ term is larger than from the vertical shift term in all models. In addition, at this level the density term exerts a considerable contribution to the increase in upwelling (of similar magnitude) in all models. A similar result is obtained for the 100 hPa material line, where only for MRI the contribution of the $\overline{w}^*$ term is weaker and to a large part cancelled by the vertical shift term, resulting in weaker positive net upwelling changes compared to the other models.

While the models agree well in their projections of net upwelling changes at 70 and 100 hPa, they can potentially miss the contribution from widening/narrowing of the upwelling region as indicated by ERA5 for the recent past. Particularly at 70 hPa the models and ERA5 differed in sign of the systematic change due to the discord in the width term contribution. However, as already mentioned the reanalyses differ substantially regarding the width changes of the upwelling region. Some reanalyses (MERRA2 and JRA55) similarly to the models do not show a systematic contribution to upwelling changes from the width term. This manifests also comparing the multi-reanalysis distribution (MRD) and multi-model distribution (MMD), both consisting of 3 members, shown in Fig. 3. Furthermore, this comparison shows that the spread of the net upwelling and individual term changes is for most parts larger for MRD than for MMD.

Figure 2. Interannual change of a net upwelling and the contributing terms at 70 hPa (top), 100 hPa (middle) and the tropopause (bottom) for the period 2015–2100. Individual models are shown with different colors. Note that the scale of the y-axis differs between the levels. Dots depict the position of the median and full lines are for the 95% credible interval. Numbers at the bottom denote the percentage occurrence of negative or positive year to year upwelling changes.

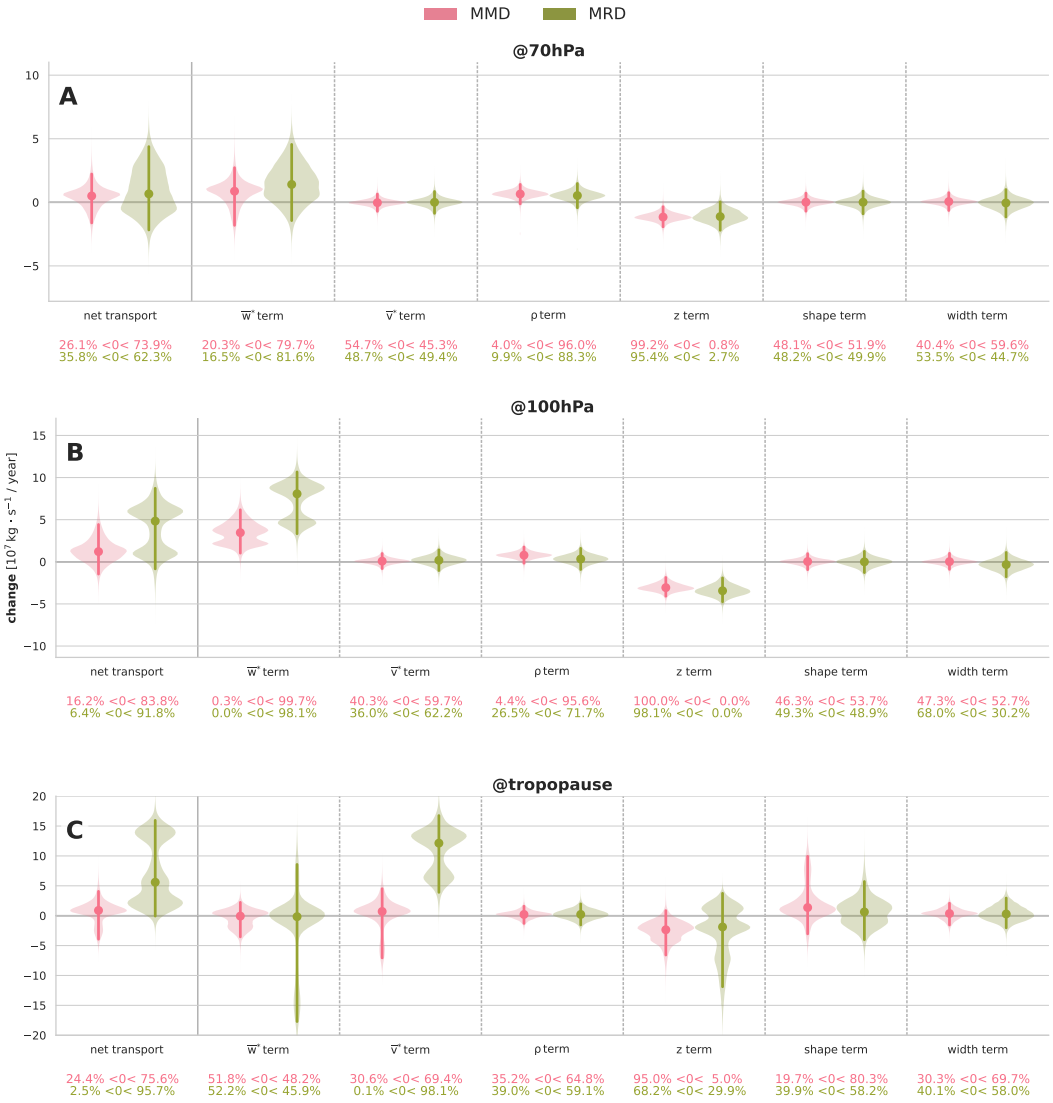

Figure 3. Interannual change of the net upwelling and the contributing terms at 70 hPa (top), 100 hPa (middle) and the tropopause (bottom) for the period 1979-2015 as in Fig. 1 but comparing the multi-model distribution (MMD: CESM2-WACCM, CESM2 and MRI-ESM2) to the multi-reanalysis distribution (MRD: ERA5, JRA55 and MERRA2).

In particular, the magnitude of the $\overline{w}^*$ term at 100 hPa and 70 hPa and magnitude of the $\overline{v}^*$ term and sign of the $\overline{w}^*$ term contribution at the TPP show a large spread (with a clear double peak structure at 100 hPa and TPP) and add considerable uncertainty to the net upwelling changes in MRD. This feature is further explored in Fig. 4, where we focus on the relationship between the changes in net transport and the $\overline{w}^*$ and width terms, respectively. In this comparison the large differences across reanalyses at all vertical levels becomes immediately apparent. Particularly, the flat relations at the TPP and 100 hPa levels for ERA5 and JRA55 stand out when compared to MERRA2, arguing for caution to attribute discrepancies between (individual) models and (individual) reanalyses.

4 Conclusions

The novel, transparent and accessible methodological framework outlined here allows to clarify the connection between structural changes of the atmosphere and the advective BDC changes and can aid to narrow down the differences and uncertainties in the advective transport among models and reanalyses. The method has obvious potential to improve matching of the simulated BDC trends with observations by triggering research towards novel constraints to date unconsidered in BDC research.

Our analysis explored for the first time advective BDC changes in full complexity, considering all relevant contributions from changes in mass flux, and the vertical and horizontal structure of the global atmosphere. Overall, our results underline that the net tropical upwelling is sensitive to all mechanisms connected to climate change, but to different amounts at different material lines and to different extent for different reanalyses and models. This includes the vertical shift and the acceleration of the circulation, as well as changes in horizontal structure influencing the widening of the upwelling region. The sensitivity of the net upwelling to these factors is enhanced by the fact that the contributions from different mechanisms can, but do not have to compensate. This makes an accurate simulation of changes in the advective BDC a daunting task for ESMs as this requires to represent all the involved mechanisms correctly (in terms of timing, strength, and amplitude).

The here identified initial constraints connected with the structural changes of the atmosphere can be directly derived from observations (vertical shift, width, and density changes) and their utilization for validating simulated BDC changes is vital, fairly straightforward and reproducible at the same time. A further important step forward towards better constraining reanalyses and global models, would be the broader availability of required ESM outputs which is suggested to be considered by the community in upcoming core variable lists for CMIP and CCMI activities.

5 Open Research

CMIP6 data can be downloaded from `https://esgf-node.llnl.gov/search/cmip6/`. ERA5 data are available from the Copernicus Climate Data Store, `https://cds.climate.copernicus.eu`. JRA55 and MERRA2 zonal mean data was obtained from S-RIP project stored at CEDA archive `https://archive.ceda.ac.uk`. The tropopause data for JRA55 can be obtained on request from Sean Davis and Susann Tegtmeier and ERA5 and MERRA2 tropopause characteristics from Lars Hoffmann. Transport and decomposition time series are stored at Zenodo, `https://doi.org/10.5281/zenodo.8099089`.

Acknowledgments
We would like to thank Sean Davis and Susann Tegtmeier for the JRA55 tropopauses and Lars Hoffmann for the ERA5 and MERRA2 tropopauses. Funding: Czech Science Foundation JUNIOR-STAR grant 23-04921M; Czech Science Foundation grant 21-03295S; Charles University, project GA UK No. 456622. AK and HR acknowledge support by the University of Natural Resources and Life Sciences, Vienna.

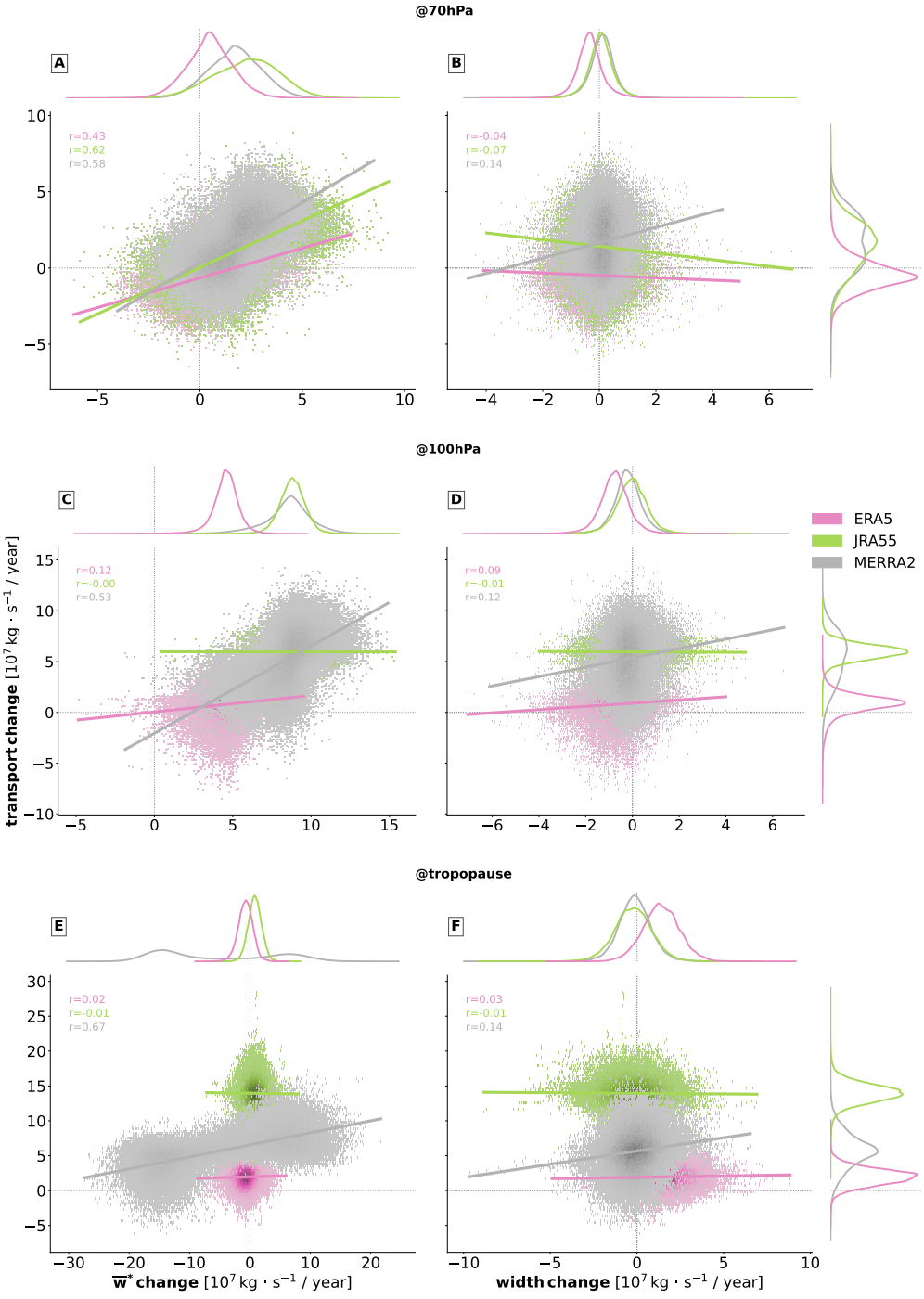

Figure 4. Interannual change of the net upwelling in relationship with $\overline{w}^*$ and width terms in the reanalyses (ERA5, JRA55, MERRA2) at 70 hPa (top), 100 hPa (middle) and the tropopause (bottom) for the period 1979-2015. Relationships between these terms shown as scatter points are quantified using linear regression (fitted lines) and correlation coefficient (annotations in upper left corners). Individual distributional side plots correspond to violin plots in Figs. 1 and 3.

References

Abalos, M., Calvo, N., Benito, S., Garny, H., Hardiman, S., Lin, P., ... Yoshida, K. (2021, 09). The brewer–dobson circulation in cmip6. *Atmospheric Chemistry and Physics*, *21*, 13571-13591. doi: 10.5194/acp-21-13571-2021

Alsing, J. (2019, 05). dlmmc: Dynamical linear model regression for atmospheric time-series analysis. *Journal of Open Source Software*, *4*, 1157. doi: 10.21105/joss.01157

Andrews, D. G., Holton, J. R., & Leovy, C. B. (1987). *Middle atmosphere dynamics*. Academic Press.

Ball, W. T., Alsing, J., Mortlock, D. J., Staehelin, J., Haigh, J. D., Peter, T., ... Rozanov, E. V. (2018). Evidence for a continuous decline in lower stratospheric ozone offsetting ozone layer recovery. *Atmospheric Chemistry and Physics*, *18*(2), 1379–1394. doi: 10.5194/acp-18-1379-2018

Berner, J., Christensen, H. M., & Sardeshmukh, P. D. (2020). Does enso regularity increase in a warming climate? *Journal of Climate*, *33*(4). doi: 10.1175/JCLI-D-19-0545.1

Bognar, K., Tegtmeier, S., Bourassa, A., Roth, C., Warnock, T., Zawada, D., & Degenstein, D. (2022). Stratospheric ozone trends for 1984–2021 in the sage ii–osiris–sage iii/iss composite dataset. *Atmospheric Chemistry and Physics*, *22*(14), 9553–9569. doi: 10.5194/acp-22-9553-2022

Butchart, N. (2014, 06). The brewer-dobson circulation. *Reviews of Geophysics*, *52*. doi: 10.1002/2013RG000448

Butchart, N., Cionni, I., Eyring, V., Shepherd, T. G., Waugh, D. W., Akiyoshi, H., ... Tian, W. (2010). Chemistry–climate model simulations of twenty-first century stratospheric climate and circulation changes. *Journal of Climate*, *23*(20). doi: 10.1175/2010JCLI3404.1

Danabasoglu, G., Lamarque, J.-F., Bacmeister, J., Bailey, D. A., DuVivier, A. K., Edwards, J., ... Strand, W. G. (2020). The community earth system model version 2 (cesm2). *Journal of Advances in Modeling Earth Systems*, *12*(2), e2019MS001916. Retrieved from `https://agupubs.onlinelibrary.wiley.com/doi/abs/10.1029/2019MS001916` doi: https://doi.org/10.1029/2019MS001916

Eichinger, R., & Šácha, P. (2020, 07). Overestimated acceleration of the advective brewer-dobson circulation due to stratospheric cooling. *Quarterly Journal of the Royal Meteorological Society*, *146*. doi: 10.1002/qj.3876

Eyring, V., Bony, S., Meehl, G. A., Senior, C. A., Stevens, B., Stouffer, R. J., & Taylor, K. E. (2016). Overview of the coupled model intercomparison project phase 6 (cmip6) experimental design and organization. *Geoscientific Model Development*, *9*(5), 1937–1958. doi: 10.5194/gmd-9-1937-2016

Gelaro, R., McCarty, W., Suárez, M. J., Todling, R., Molod, A., Takacs, L., ... Zhao, B. (2017). The modern-era retrospective analysis for research and applications, version 2 (merra-2). *Journal of Climate*, *30*(14), 5419 - 5454. Retrieved from `https://journals.ametsoc.org/view/journals/clim/30/14/jcli-d-16-0758.1.xml` doi: https://doi.org/10.1175/JCLI-D-16-0758.1

Hardiman, S., Butchart, N., & Calvo, N. (2014, 07). The morphology of the brewer–dobson circulation and its response to climate change in cmip5 simulations. *Quarterly Journal of the Royal Meteorological Society*, *140*. doi: 10.1002/qj.2258

Hersbach, H., Bell, B., Berrisford, P., Hirahara, S., Horányi, A., Muñoz-Sabater, J., ... Thépaut, J. (2020). The era5 global reanalysis. *Quarterly Journal of the Royal Meteorological Society*, *146*(730), 1999-2049. doi: 10.1002/qj.3803

Iglesias-Suarez, F., Wild, O., Kinnison, D. E., Garcia, R. R., Marsh, D. R., Lamarque, J.-F., ... Young, P. J. (2021). Tropical stratospheric circulation and ozone coupled to pacific multi-decadal variability. *Geophysical Research Letters*, *48*(11), e2020GL092162. doi: 10.1029/2020GL092162

Ivy, D., Solomon, S., Calvo, N., & Thompson, D. (2017, February 1). Observed connections of arctic stratospheric ozone extremes to northern hemisphere surface climate. *Environmental Research Letters*, *12*(2). doi: 10.1088/1748-9326/aa57a4

Karagodin-Doyennel, A., Rozanov, E., Sukhodolov, T., Egorova, Sedlacek, J., Ball, W., & Peter, T. (2022). The historical ozone trends simulated with the socolv4 and their comparison with observations and reanalysis. *EGUsphere*, *2022*, 1–26. doi: 10.5194/acp-22-15333-2022

Karpechko, A., Maycock, A., Abalos, M., Akiyoshi, H., Arblaster, J., Garfinkel, C., ... Son, S.-W. (2018, 01). Scientific assessment of ozone depletion: 2018, chapter 5: Stratospheric ozone changes and climate.

Kobayashi, S., Ota, Y., Harada, Y., Ebita, A., Moriya, M., Onoda, H., ... Takahashi, K. (2015, 02). The jra-55 reanalysis: General specifications and basic characteristics. *Journal of the Meteorological Society of Japan*, *93*, 5-48. doi: 10.2151/jmsj.2015-001

Kuchar, A., Ball, W. T., Rozanov, E. V., Stenke, A., Revell, L., Miksovsky, J., ... Peter, T. (2017). On the aliasing of the solar cycle in the lower stratospheric tropical temperature. *Journal of Geophysical Research: Atmospheres*, *122*(17), 9076-9093. doi: 10.1002/2017JD026948

Laine, M., Latva-Pukkila, N., & Kyrölä, E. (2014). Analysing time-varying trends in stratospheric ozone time series using the state space approach. *Atmospheric Chemistry and Physics*, *14*(18), 9707–9725. doi: 10.5194/acp-14-9707-2014

Lübken, F.-J., Berger, U., & Baumgarten, G. (2013, 12). Temperature trend in the midlatitude summer mesosphere. *Journal of Geophysical Research: Atmospheres*, *118*. doi: 10.1002/2013JD020576

Maillard Barras, E., Haefele, A., Stübi, R., Jouberton, A., Schill, H., Petropavlovskikh, I., ... Froidevaux, L. (2022). Dynamical linear modeling estimates of long-term ozone trends from homogenized dobson umkehr profiles at arosa/davos, switzerland. *Atmospheric Chemistry and Physics*, *22*(21), 14283–14302. doi: 10.5194/acp-22-14283-2022

Oberländer-Hayn, S., Gerber, E. P., Abalichin, J., Akiyoshi, H., Kerschbaumer, A., Kubin, A., ... Oman, L. D. (2016). Is the brewer-dobson circulation increasing or moving upward? *Geophysical Research Letters*, *43*(4), 1772-1779. Retrieved from `https://agupubs.onlinelibrary.wiley.com/doi/abs/10.1002/2015GL067545` doi: https://doi.org/10.1002/2015GL067545

Ortland, D., & Alexander, M. (2014, 03). The residual-mean circulation in the tropical tropopause layer driven by tropical waves. *Journal of the Atmospheric Sciences*, *71*. doi: 10.1175/JAS-D-13-0100.1

Pisoft, P., Sacha, P., Polvani, L. M., Añel, J. A., de la Torre, L., Eichinger, R., ... Rieder, H. E. (2021, may). Stratospheric contraction caused by increasing greenhouse gases. *Environmental Research Letters*, *16*(6), 064038. doi: 10.1088/1748-9326/abfe2b

Polvani, L. M., Abalos, M., Garcia, R., Kinnison, D., & Randel, W. J. (2018). Significant weakening of brewer-dobson circulation trends over the 21st century as a consequence of the montreal protocol. *Geophysical Research Letters*, *45*(1), 401-409. Retrieved from `https://agupubs.onlinelibrary.wiley.com/doi/abs/10.1002/2017GL075345` doi: https://doi.org/10.1002/2017GL075345

Randel, W., & Park, M. (2019, 07). Diagnosing observed stratospheric water vapor relationships to the cold point tropical tropopause. *Journal of Geophysical Research: Atmospheres*, *124*. doi: 10.1029/2019JD030648

Santer, B. D., Po-Chedley, S., Zhao, L., Zou, C.-Z., Fu, Q., Solomon, S., ... Taylor, K. E. (2023). Exceptional stratospheric contribution to human fingerprints on atmospheric temperature. *Proceedings of the National Academy of Sciences*, *120*(20), e2300758120. Retrieved from `https://www.pnas.org/doi/abs/10.1073/pnas.2300758120` doi: 10.1073/pnas.2300758120

Santer, B. D., Wehner, M. F., Wigley, T. M. L., Sausen, R., Meehl, G. A., Taylor, K. E., ... Brüggemann, W. (2003). Contributions of anthropogenic and natural forcing to recent tropopause height changes. *Science*, *301*(5632), 479-483. Retrieved from `https://www.science.org/doi/abs/10.1126/science.1084123` doi: 10.1126/science.1084123

Sellar, A. A., Walton, J., Jones, C. G., Wood, R., Abraham, N. L., Andrejczuk, M., ...

Griffiths, P. T. (2020). Implementation of u.k. earth system models for cmip6. *Journal of Advances in Modeling Earth Systems*, *12*(4), e2019MS001946. Retrieved from https://agupubs.onlinelibrary.wiley.com/doi/abs/10.1029/2019MS001946 (e2019MS001946 10.1029/2019MS001946) doi: https://doi.org/10.1029/2019MS001946

Shepherd, T., & McLandress, C. (2011, 04). A robust mechanism for strengthening of the brewer-dobson circulation in response to climate change: Critical-layer control of subtropical wave breaking. *Journal of The Atmospheric Sciences - J ATMOS SCI*, *68*, 784-797. doi: 10.1175/2010JAS3608.1

Solomon, S., Liu, H., Marsh, D., McInerney, J., Qian, L., & Vitt, F. (2018, 01). Whole atmosphere simulation of anthropogenic climate change. *Geophysical Research Letters*, *45*. doi: 10.1002/2017gl076950

Staten, P., Grise, K., Davis, S., Karnauskas, K., Waugh, D., Maycock, A., ... Son, S.-W. (2020, 02). Tropical widening: From global variations to regional impacts. *Bulletin of the American Meteorological Society*, *101*. doi: 10.1175/BAMS-D-19-0047.1

Stiller, G. P., Fierli, F., Ploeger, F., Cagnazzo, C., Funke, B., Haenel, F. J., ... von Clarmann, T. (2017). Shift of subtropical transport barriers explains observed hemispheric asymmetry of decadal trends of age of air. *Atmospheric Chemistry and Physics*, *17*(18), 11177–11192. doi: 10.5194/acp-17-11177-2017

Vallis, G., Zurita-Gotor, P., Cairns, C., & Kidston, J. (2014, 11). Response of the large-scale structure of the atmosphere to global warming. *Quarterly Journal of the Royal Meteorological Society*, *141*. doi: 10.1002/qj.2456

WMO, W. M. O. (2018). Scientific assessment of ozone depletion: 2018, global ozone research and monitoring project – report no. 58, 588 pp.

Yukimoto, S., Kawai, H., Koshiro, T., Oshima, N., Yoshida, K., URAKAWA, S., ... ISHII, M. (2019, 06). The meteorological research institute earth system model version 2.0, mri-esm2.0: Description and basic evaluation of the physical component. *Journal of the Meteorological Society of Japan*, *97*. doi: 10.2151/jmsj.2019-051

Šácha, P., Eichinger, R., Garny, H., Pisoft, P., Dietmüller, S., de la Torre Ramos, L., ... Añel, J. (2019, 06). Extratropical age of air trends and causative factors in climate projection simulations. *Atmospheric Chemistry and Physics*, *19*, 7627-7647. doi: 10.5194/acp-19-7627-2019